Uptake Measurements of Acetaldehyde on Solid Ice Surfaces and on Solid/Liquid Supercooled Mixtures Doped with HNO3 in the Temperature Range 203-253 K

3 AUTHORS, INCLUDING:

Stéphane Le Calvé

French National Centre for Scientific Resea…

90 PUBLICATIONS   **994** CITATIONS

Uptake Measurements of Acetaldehyde on Solid Ice Surfaces and on Solid/Liquid Supercooled Mixtures Doped with HNO₃ in the Temperature Range 203−253 K

M. Petitjean, Ph. Mirabel, and S. Le Calvé*

Laboratoire des Matériaux, Surfaces et Procédés pour la Catalyse (LMSPC, UMR 7515 CNRS/UDS), 25 rue Becquerel, 67087 Strasbourg Cedex 02, France

Received: November 18, 2008; Revised Manuscript Received: January 13, 2009

Uptake of acetaldehyde on ice surfaces has been investigated over the temperature range 203−253 K using a coated wall flow tube coupled to a mass spectrometric detection. The experiments were conducted on pure ice surfaces and on liquid/solid ice mixture both doped with nitric acid (0.063, 0.63, and 6.3 wt %). Uptake of acetaldehyde on these surfaces was always found to be totally reversible whatever the experimental conditions were. The number of acetaldehyde molecules adsorbed per surface unit was conventionally plotted as a function of acetaldehyde concentration in the gas phase. Although the amounts of acetaldehyde adsorbed on solid ice surfaces (pure and HNO₃-doped ice) were approximately similar and rather limited, the number of acetaldehyde molecules taken up on the HNO₃-doped solid ice/liquid mixtures are significantly higher, up to 1 or 2 orders of magnitudes compared to pure ice surfaces. At 213 K for example and for low concentrations of acetaldehyde ($<1 \times 10^{13}$ molecule cm^{-3}), the amount of acetaldehyde molecules taken up on solid/liquid doped surfaces is 3.3 and 8.8 times higher than those measured on pure ice respectively for 0.063 and 0.63 wt % of HNO₃. The huge quantities of acetaldehyde taken up by liquid-/solid-doped mixtures are likely dissolved in the nonhomogeneous liquid part of the surfaces according to the Henry's law equilibrium. As a consequence, up to about 10% of acetaldehyde may be scavenged by supercooled liquid droplets of convective clouds in the upper troposphere.

Introduction

The upper troposphere (UT) is characterized by low temperatures ranging from about 188 to 233 K and by the presence of ice (cirrus) as well as mixed ice/water clouds covering a substantial portion (up to 25%) of the Earth's surface.[1] Ice clouds are formed in the troposphere at altitudes of 4−15 km where they can reflect the incoming solar radiation and trap the terrestrial infrared radiation. Depending on the dominant effect, this results either in a cooling or a warming of the underlying layers of air, according to the particle density, their morphology, and their (surface) chemical composition. The change of their frequency and distribution, therefore, impacts substantially on the regional and global climate.

The interaction between trace gases and mixed or ice clouds can promote heterogeneous chemistry and therefore initiate the transfer of chemical species from the gas into the condensed phases. Hydrometeors hence appear to offer a favorable environment for fast physical and chemical transformations, which can modify both trace gas and aerosol compositions.[2] Below approximately 230 K, clouds are predominantly composed of ice crystals with number densities in the range of 0.001−50 cm^{-3}.[1,3] However, even at temperature as low as 230 K, clouds composed of supercooled liquid water droplets have also been observed either in mixed clouds containing both ice crystals and supercooled droplets[4] or in deep convective clouds where most of the condensed water remained liquid down to 235 K with densities up to 1.8 g m^{-3}.[5]

Vertical advective transport influences the concentration and vertical distribution of trace gases and hence the oxidation capacity in the troposphere. Deep convection can rapidly transport anthropogenic pollutants such as NO$_x$, VOCs, and HO$_x$ precursors from the planetary boundary layer (PBL) into the upper troposphere,[6] where they can participate to the local photochemistry and modify the ozone concentration. During the convection, soluble pollutants including nitric acid, alcohols, carbonyl compounds, and carboxylic acids are likely to be scavenged by supercooled droplets contained in polluted convective air masses.[7] When these supercooled droplets freeze, the dissolved species are retained in the bulk of these new ice particles [8,9] until these latter evaporate once in the UT.

As a consequence of convection, Laaksonen et al. [10] observed correlated high mixing ratios of both acetone and nitric acid in the UT suggesting that these air masses had recent contact with the polluted PBL. The presence of oxygenated volatile organic compounds (OVOCs) such as alcohols, aldehydes, ketones, and carboxylic acids in the UT is also well established.[11−14] The photolysis of carbonyl compounds such as aldehydes and ketones in the UT is a net source of HO$_x$ (OH + HO₂) and hence leads to an enhanced abundance of these oxidants as well as of peroxyacetyl nitrate (PAN). Enhanced production of main oxidants of the atmosphere can then affect the concentrations of many other trace gases and is likely to modify the ozone cycling reactions in this region, whereas PAN, as a relative long-lived NO$_x$ reservoir, can transport nitrogen oxides from one region of the atmosphere to another.

Whereas the effect of the OVOCs on the chemistry of the UT is in principle reasonably understood, it is far from being quantifiable. The uncertainties result mainly from the presence of ice or liquid/ice clouds that tends to modify the gas-phase concentrations of the OVOCs due to their dissolution in supercooled droplets and to their adsorption on ice surfaces. Because of the particular relevance of carbonyl compounds on

* To whom correspondence should be addressed. Fax: +33-(0)3-90-24-04-02. E-mail: slecalve@unistra.fr.

the HO$_x$/oxidants level of the gas phase, their participation in surface/droplet chemistry is of particular relevance.[15]

As has been shown by model calculation, [8,10,16] the presence of trace constituents, such as nitric acid, may substantially modify supercooled droplets formation at temperature above 233 K, affecting both their size and number concentrations. Tropospheric mixing ratios of nitric acid vary typically between 0.1 and 2.0 ppb for altitude range of 5−13 km,[10] that is in both the mid and upper troposphere. The partitioning of nitric acid in ice clouds is still not well understood, although it is an important parameter to understand the vertical redistribution of HNO$_3$ in the UT.[8] Up to now, most of the models have considered only equilibrium adsorption of HNO$_3$ by cloud particles to describe the formation of mixed HNO$_3$/H$_2$O particles as observed in cirrus clouds. However, the ice surfaces are often not in equilibrium but are continuously growing and evaporating due to temperature fluctuations. Therefore, nitric acid can be efficiently trapped in the bulk during the growth phase.[8,9,16] On the basis of this idea, the model of Krämer and co-workers[10] results in concentrations of HNO$_3$ in ternary (HNO$_3$−H$_2$SO$_4$−H$_2$O) and quaternary (NH$_3$−HNO$_3$−H$_2$SO$_4$−H$_2$O) solutions ranging, respectively, from 0.04 to 17 wt % and 1.2 to 41 wt % for temperatures between 213 and 223 K, relative humidities between 100 and 160%, and initial gaseous HNO$_3$ mixing ratio between 0.05 and 1.7 ppb.

Recent laboratory studies on OVOCs have focused on the adsorption of these oxygenated VOCs (alcohols, acetic acid, acetone, etc.) on pure ice surfaces. The results have highlighted that, even if the interaction between the organic compounds and pure ice is strong enough to lead to a monolayer adsorption in laboratory experiments,[17−22] the occurrence of cirrus clouds in the UT region will not affect significantly the gas phase concentrations of oxygenated organic compounds. The question remains, however, to know what happens if instead of pure ice one considers ice doped with strong acids (H$_2$SO$_4$ and HNO$_3$), which is more representative for the UT region of the atmosphere. Whereas the amount of adsorbed organic molecules on pure ice is always limited, recent studies have shown that the amount of acetone and ethanol taken up by supercooled solutions doped with nitric acid is 1 or 2 orders of magnitude higher than those observed on pure ice.[7,23]

In ice and liquid/ice clouds, oxygenated VOCs interact with supercooled droplets or ice crystals according to several coupled processes. In the present work, we aim at a better characterization of the first step, that is adsorption of acetaldehyde on ice or dissolution in supercooled solution, for temperatures encountered in both the mid and upper troposphere, that is between 203 and 253 K. The adsorption of acetaldehyde on pure ice surfaces has already been investigated for temperatures below 180 K by Hudson et al.[24] These authors did not observe any uptake of acetaldehyde on an ice film with a HNO$_3$ monolayer coverage, on a supercooled 4:1 HNO$_3$/H$_2$O solution nor on a NAT film, from 190 to 200 K.

To our knowledge, this work is nevertheless the first to report uptake of acetaldehyde on liquid/ice and ice surfaces for temperature and nitric acid content relevant of the mid and upper troposphere. Our experimental data were then used to estimate the partitioning of oxygenated VOCs in ice and liquid/ice clouds.

Experimental Section

The uptake of acetaldehyde on ice and liquid/ice surfaces was studied using a vertical coated wall flow tube coupled to a mass spectrometer, already described elsewhere.[7,18,19,23] We will therefore provide only a brief summary of its principle operation.
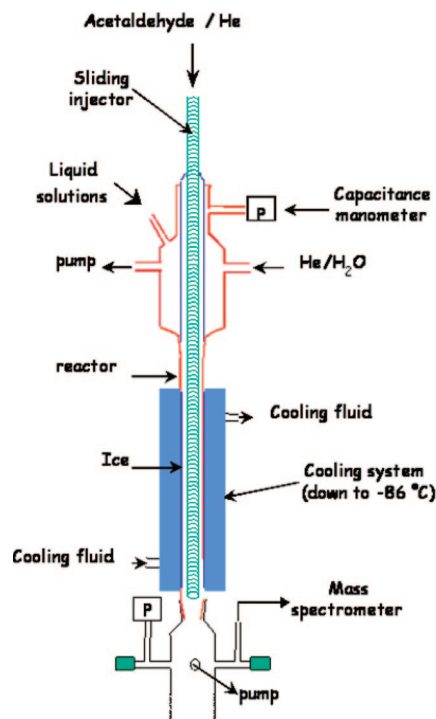

Figure 1. Schematic illustration of the vertical coated wall flow tube.

The apparatus, which is shown in Figure 1, has a double jacket to allow the system to be operated at low temperature. The cooling fluid was circulated in the inner jacket from a cooler/circulator (Huber, Unistat 385), while vacuum was maintained in the outer jacket for thermal insulation. The temperature of the flow tube could be cooled down and regulated between 188 and 253 K.

The jacketed flow tube was approximately 40 cm in length with an internal diameter of 2.8 cm. The ice surface was prepared by totally wetting, with either Milli-Q water (18 MΩ cm) or solutions containing HNO$_3$ (0.063, 0.63, and 6.3 wt %), and the inner wall of the flow tube that was precooled to 263 K. The viscous aqueous film was then cooled down to 253 K to obtain a solid or liquid/solid film that can be retained during the course of the experiments. Finally, the film was either cooled directly to the desired temperature over a period of 10−15 min or cooled to 188 K and then warmed to the desired temperature. The thickness of the ice film was estimated between 40 and 110 μm by weighing the resulting liquid water when the ice film was melted at the end of the experiment.

The helium carrier gas (UHP certified to >99.9995% from Messer) was used without further purification. During the experiment, water vapor was added to the main helium flow to provide a partial pressure of water, equal to the vapor pressure of water over the ice film, and therefore inhibit net evaporation of this film. The resulting humidified helium flow was injected at the upstream end of the flow reactor.

Acetaldehyde (≥99%) purchased from Fluka was further purified before being used by repeated freeze, pump, and thaw cycles as well as by fractional distillation. To perform an experiment, acetaldehyde was premixed with helium in a 10 L glass light-tight bulb to form 2.3×10^{-2} to 6.1% mixtures, at a total pressure of ∼740−770 Torr. The mixture containing acetaldehyde was injected into the flow tube reactor via a sliding injector (Figure 1) that allows changing the exposed ice or liquid/ice surfaces (130−220 cm^2). The injector was jacketed

Uptake Measurements of Acetaldehyde

J. Phys. Chem. A, Vol. 113, No. 17, 2009 **5093**
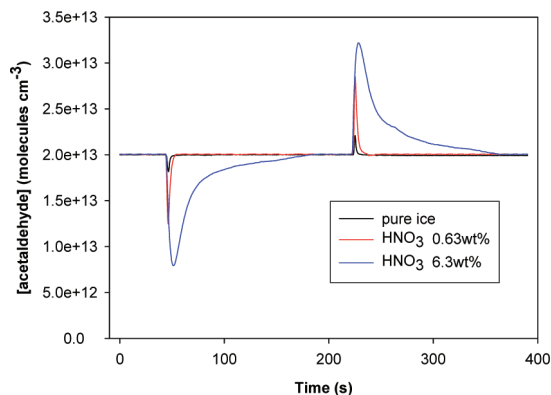
Figure 2. Acetaldehyde concentrations in the gas phase as a function of time during the adsorption of acetaldehyde on different ice surfaces at 213 K (with [acetaldehyde]$_{\text{gas phase}}$ = 1.87, 2.01, and 1.88 × 10^{13} molecules cm^{-3} for respectively pure ice, HNO$_3$ 0.63 wt %, and HNO$_3$ 6.3 wt %).

Figure 3. Adsorption isotherms of acetaldehyde on pure ice surfaces at 203, 213, 223, 233, 243, and 253 K (logarithmic scale). The solid lines correspond to the Langmuir's fits according to eq 1 for 203, 213, and 223 K (text).

and a heating tape was wound up in the jacket to ensure a gentle heating of the injector.[19]

All of the gases flowed into the reactor through Teflon tubing. The gas mixture containing acetaldehyde and water vapor diluted in helium was flowed through the reactor with a linear velocity ranging between 30 and 100 cm s^{-1}. Concentrations of acetaldehyde in the gas phase were calculated from their mass flow rates, temperature, and pressure in the flow tube. All the flow rates were controlled and measured with calibrated mass flowmeters (Millipore, 2900 series). The pressure that ranged between 1.9 and 2.5 Torr was measured with two capacitance manometers (Edwards, 622 barocel range 0−100 Torr and Keller, PAA−41 range 0−76 Torr) connected at the top and bottom of the flow tube. Under our experimental conditions, the mixing time τ_{mix} between acetaldehyde flow, and the main He flow was lower than 2 ms,[25] which corresponds to a mixing length smaller than 0.3 cm.

The gas stream coming out of the flow tube was analyzed using a differentially pumped mass quadruple spectrometer Pfeiffer Vacuum QMS. Acetaldehyde was monitored at the main fragment ion CH$_3$CO$^+$ peak at m/z = 43 amu using a temporal resolution of 30 ms, an ionization energy of 70 eV and an emission current of 1000 μA.

Results and Discussion

Uptake experiments were performed by first establishing a highly stable flow of acetaldehyde in the injector, this injector being positioned past the end of ice film. The injector was then moved quickly to an upstream position so that the ice film was exposed to acetaldehyde. The uptake of acetaldehyde on the ice film leads to a drop of signal as shown in Figure 2. After a time scale ranging from a few seconds to several minutes depending on the investigated ice surface, the ice surface was then saturated and the MS-signal returned to its initial level. When the injector was pushed back, acetaldehyde desorbed from the ice surface and the signal increased and then again returned to its initial level. Similar experiments were conducted for various ice surfaces (pure ice or doped-ice surfaces) over a temperature range of 203−253 K and for gas-phase concentrations varying from 5.7 × 10^{11} to 8.25 × 10^{14} molecules cm^{-3}.

Adsorption on Pure Ice Surfaces. *Surface Coverage.* The number of acetaldehyde molecules adsorbed N_{ads} on the ice surface was determined from the integrated area of the adsorption peak (in molecule s cm^{-3}) and the total flow rate in the flow tube (cm^3 s^{-1}). The surface coverage N (in molecule cm^{-2})
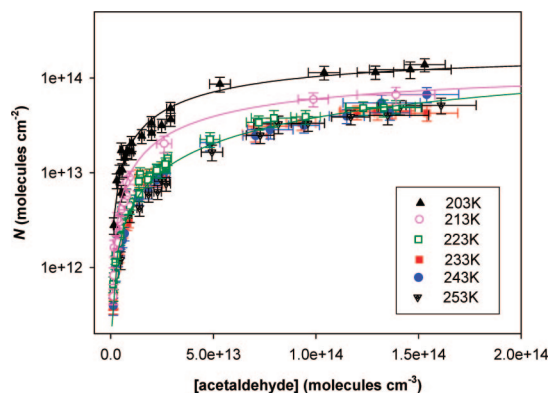
of acetaldehyde was then calculated from the geometric exposed ice surface area S_{ice} (in cm^2) according to $N = N_{\text{ads}}/S_{\text{ice}}$. The experiments were performed several times using newly generated ice surfaces to ensure the reproducibility of the data.

Surface coverage N versus gas phase concentrations has been plotted in Figure 3 for six temperatures: 203, 213, 223, 233, 243, and 253 K. The relative errors on the gas-phase concentrations, which range between 6 and 16% (horizontal error bars in this figure), have been calculated from the possible uncertainties on each flow, total pressure, etc. The quoted errors on N (vertical error bars) arise from uncertainties made on the total flow rate, exposed ice area, and concentrations in the gas phase. They also include a systematic 2% error that corresponds to the error on the integrated area of adsorption peaks. These resulting errors on N vary between 14 and 23%.

Langmuir Isotherms. Langmuir's theory, which has the main assumption that adsorption cannot proceed beyond monolayer coverage, was used to analyze our experimental data. According to this theory, the number of molecules adsorbed per unit area of ice surface is related to the concentration of acetaldehyde in the gas phase. Eq 1 states this dependence:

$$\theta = \frac{N}{N_{\text{M}}} = \frac{K_{\text{ads}}(T)[\text{acetaldehyde}]_{\text{gas}}}{1 + K_{\text{ads}}(T)[\text{acetaldehyde}]_{\text{gas}}} \quad (1)$$

where θ is the fractional coverage, N_{M} is the monolayer capacity (in molecule cm^{-2}), and $K_{\text{ads}}(T)$ is the temperature dependent adsorption constant that describes partitioning between adsorbed and nonadsorbed molecules (cm^3 molecule^{-1}).

From a thermodynamic point of view, the equilibrium between the gas and the surface can also be expressed by using a dimensionless partition coefficient, K:

$$\frac{N}{[\text{acetaldehyde}]_{\text{gas}}} \times \frac{A}{V} = \exp\left(\frac{\Delta G^0_{\text{ads}}}{RT}\right) = K \quad (2)$$

where R is the perfect gas constant, A/V is the area-to-volume ratio (cm^{-1}) of an ideal gas adsorbed at the surface, and ΔG^0_{ads} is the free energy of adsorption. A/V defines the standard state for the adsorbed phase. In absence of general agreement on the choice of a standard state, the ratio of A/V was conveniently considered equal to ∼1.7 × 10^7 cm^{-1},[26,27] which corresponds to a molar area of 3.74 × 10^7 m^2 mol^{-1}. Note that the enthalpy does not depend on the choice of standard states.[28] The
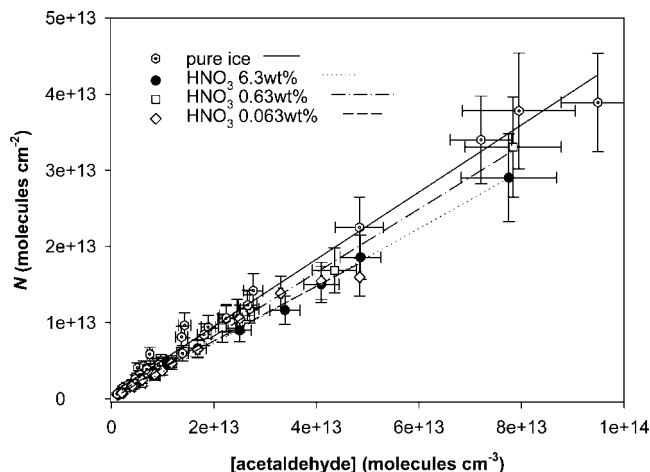
Figure 4. Linear isotherms of acetaldehyde on different type of solid ice surfaces at 223 K. The lines correspond to the linear fits (eq 5).

advantage of the chosen standard state is its independence of temperature, particle size, and absolute values of both V and A.[29]

ΔG^0_{ads} is, as usual, related to the enthalpy and entropy of adsorption via the Gibb's equation:

$$\Delta G^0_{ads} = \Delta H^0_{ads} - T\Delta S^0_{ads} = -RT\ln K(T) \quad (3)$$

At low concentration, $K_{ads}(T)$ [acetaldehyde]$_{gas} \ll 1$ in eq 1, so that K is related to K_{ads} as follows:

$$K_{ads}(T) \times N_M = K(T) \times \frac{V}{A} \quad (4)$$

In addition, N increases linearly with the concentration of acetaldehyde with a slope $N_M K_{ads}(T)$ or $K(T) \times V/A$ according to:

$$N = K_{ads}(T) \times N_M \times [\text{acetaldehyde}]_{gas}$$

$$= K(T) \times \frac{V}{A} \times [\text{acetaldehyde}]_{gas} \quad (5)$$

The data collected at 203, 213, and 223 K were used for the Langmuir's analysis and were fitted according to eq 1 as shown in Figure 3 considering both N_M and K_{ads} as free parameters. The resulting values for the Langmuir constants K_{ads} are (in units of 10^{-15} cm^3 molecule^{-1}): K_{ads} (203 K) = 12.0 $\pm$ 2.6, K_{ads} (213 K) = 7.9 $\pm$ 1.7, and K_{ads} (223 K) = 5.0 $\pm$ 1.0. The monolayer capacities N_M are 1.90 $\pm$ 0.20, 1.32 $\pm$ 0.13, and 1.26 $\pm$ 0.15 in units of 10^{14} molecule cm^{-2} at 203, 213, and 223 K, respectively. Although a higher value of N_M was found at 203 K, probably due to the presence of cracks leading to a higher surface area of our ice samples, no significant variation of N_M with temperature was found between 213 and 223 K so that an average value $N_M = (1.3 \pm 0.2) \times 10^{14}$ molecules cm^{-2} has been calculated. Both values of N_M and $K_{ads}(T)$ can be used.

Besides, Figure 4 shows a typical linear isotherm on pure ice of N versus [acetaldehyde]$_{gas}$ at 223 K. The resulting values of both $K(T)$ and $K_{ads} \times N_M$ are derived from the slope of this plot according to eq 5 and are reported in Table 1. For each temperature, ΔG^0_{ads} can be obtained from eq 3, although ΔH^0_{ads} can be calculated from eq 3 when ΔS^0_{ads} is fixed from Trouton's

rule[30] (the errors bars are given at 2σ level and include experimental error that can be estimated to approximately 5%). The temperature dependence of $K(T)$ between 203 and 253 K was then used to determine the adsorption enthalpy ΔH_{ads} of acetaldehyde on pure ice, according to eq 3.

Both values of N_M and $K_{ads}(T)$ derived from Langmuir's model can be used to determine $K(T)$ by applying eq 4. As shown in figure 5, the values of K derived by Langmuir model are in very good agreement with those obtained by linear fit at low acetaldehyde concentrations. Besides, the plot of ln K versus $1/T$ is linear for the temperature range 203–223 K, although for temperature above 233 K, values start to deviate due to the likely presence of a quasi-liquid layer on the pure ice surface. The resulting adsorption enthalpy of acetaldehyde on ice between 203 and 233 K, obtained by linear weighted least-squares fitting, is $\Delta H_{ads} = -16$ (± 3) kJ mol^{-1} (the quoted errors are given at 2σ level + 5%). However, this value of ΔH_{ads} is higher than the enthalpy of condensation − 30.3 kJ mol^{-1} obtained according to the Lyman's method,[31] which is not thermodynamically consistent. Therefore, a second approach has been applied to the data where ΔS_{ads} was set to be −87.3 J K^{-1} mol^{-1} according to the Trouton's rule.[30] The resulting values for ΔH_{ads} are the following (in units of kJ mol^{-1}): − 36.4 $\pm$ 2.0 (203 K), − 38.9 $\pm$ 2.1 (213 K), − 41.6 $\pm$ 2.3 (223 K).

Comparison with Previous Studies. Our value for $N_M = (1.3 \pm 0.2) \times 10^{14}$ molecules cm^{-2} is consistent with the upper limit ($<4 \times 10^{14}$ molecules cm^{-2}) previously reported by Hudson et al. (2002) for temperature ranging between 120 and 180 K. Similarly, our value of the adsorption enthalpy $\Delta H_{ads} = -42 \pm 4$ kJ mol^{-1} compares favorably with their determination also obtained with the Trouton's rule; namely $\Delta H_{ads} = -34.7$ kJ mol^{-1}.[24]

Uptake on Solid Ice or Solid/Liquid Surfaces Doped with HNO₃. Experiments were conducted on solid or solid/liquid ice films doped with HNO₃ (0.01, 0.1, and 1 N, which correspond to 0.063, 0.63, and 6.3 wt % of HNO₃) at temperatures ranging from 203 to 253 K. These temperatures and nitric acid concentrations were chosen to mimic the conditions that have been encountered in either cirrus clouds [32–34] or mixed clouds where supercooled droplets can persist down to 233K.
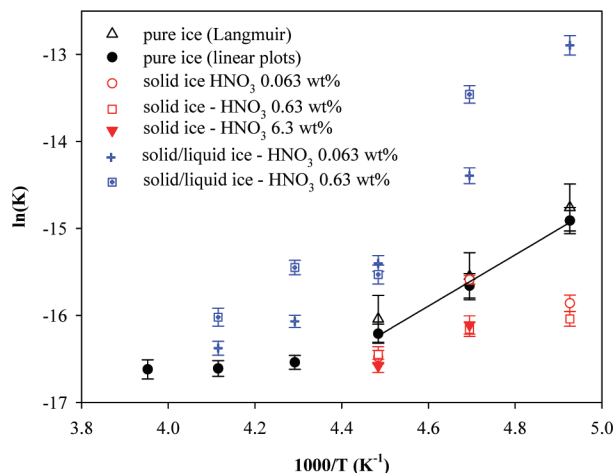
Adsorption on Solid Ice Surfaces Doped with HNO₃. Our coated solid/liquid ice film was prepared at ∼253 K and cooled down to very low temperature, typically at 185 K in our experiments. This method ensures to obtain a solid phase (ice + β-NAT) according to the dynamic phase diagram (as opposed to the equilibrium phase diagram) reported by Mahé (1999), in which the part containing both solid and liquid phases persists down to 191.4–197.3 K depending on the amount of nitric acid (Figure 6). Recall that, in the case of a dynamic phase diagram, liquid/solid supercooled mixtures can be observed below the solidus line determined at equilibrium state. Once obtained, the solid-doped ice surface was then heated to the desired temperature. The HNO₃/H₂O equilibrium phase diagram[35] shows that for temperatures below 230 K we were operating in the solid domain (Figure 6), whereas temperatures above 230 K correspond to the liquid−solid domain.

Again, adsorption of acetaldehyde was always reversible under our experimental conditions whatever the concentration of HNO₃, suggesting that no reaction occurs between acetaldehyde and nitric acid except the probable partial protonation of acetaldehyde following a well-known equilibrium. According to eq 5, the resulting values of K are derived from the linear isotherms and are reported in both Table 1 and Figure 4.

Uptake Measurements of Acetaldehyde

J. Phys. Chem. A, Vol. 113, No. 17, 2009 **5095**

TABLE 1: Values of $N_M \times K_{ads}(T)$, $K(T)$, ΔG^0_{ads}, and ΔH^0_{ads} for Different Types of Solid Ice Surfaces at 203, 213, 223, 233, 243, and 253 K[a]

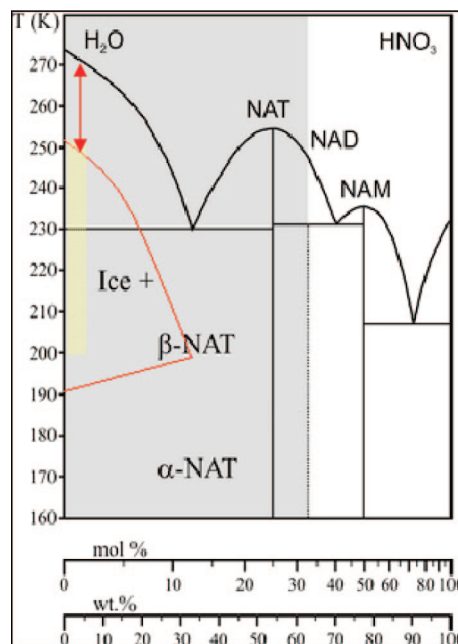| T (K)	$N_M \times K_{ads}$ (cm)[b]	linearity domain up to	R^{2b}	$K \times 10^{-8}$(dimensionless)[c]	$-\Delta G^0_{ads}$ (kJ mol^{-1})[d]	$-\Delta H^0_{ads}$ (kJ mol^{-1})
			Pure Ice			
203	2.08 ($\pm$0.19)	1.2×10^{13}	0.99	35.3 ($\pm$3.3)	25.1 ($\pm$1.1)	35.4 ($\pm$1.7)
213	0.95 ($\pm$0.09)	1.2×10^{13}	0.98	16.2 ($\pm$1.5)	27.7 ($\pm$1.3)	38.6 ($\pm$1.8)
223	0.46 ($\pm$0.04)	1×10^{14}	0.99	7.7 ($\pm$0.7)	30.4 ($\pm$1.5)	41.8 ($\pm$2.0)
233	0.39 ($\pm$0.03)	1×10^{14}	0.99	6.5 ($\pm$0.6)	32.0 ($\pm$1.5)	44.0 ($\pm$2.1)
243	0.36 ($\pm$0.03)	1×10^{14}	0.99	6.1 ($\pm$0.6)	33.6 ($\pm$1.6)	46.0 ($\pm$2.2)
253	0.35 ($\pm$0.04)	1×10^{14}	0.99	6.0 ($\pm$0.6)	35.0 ($\pm$1.6)	48.0 ($\pm$2.2)
		Solid Ice Doped with 0.063 wt % of HNO$_3$				
203	0.76 ($\pm$0.07)	4×10^{13}	0.99	12.9 ($\pm$1.2)	26.8 ($\pm$1.3)	37.2 ($\pm$1.6)
213	1.00 ($\pm$0.05)	4×10^{13}	1	17.0 ($\pm$0.8)	27.6 ($\pm$1.4)	39.7 ($\pm$1.9)
223	0.41 ($\pm$0.03)	4×10^{13}	0.99	7.0 ($\pm$0.5)	30.5 ($\pm$1.5)	42.1 ($\pm$2.0)
		Solid Ice Doped with 0.63 wt % of HNO$_3$				
203	0.64 ($\pm$0.05)	8×10^{13}	0.99	10.85 ($\pm$0.9)	27.1 ($\pm$1.3)	37.4 ($\pm$1.8)
213	0.56 ($\pm$0.05)	5×10^{13}	0.99	9.60 ($\pm$0.8)	28.6 ($\pm$1.4)	39.5 ($\pm$1.9)
223	0.42 ($\pm$0.04)	5×10^{13}	0.98	7.16 ($\pm$0.6)	30.5 ($\pm$1.4)	41.9 ($\pm$2.0)
		Solid Ice Doped with 6.3 wt % of HNO$_3$				
213	0.59 ($\pm$0.06)	9×10^{13}	0.99	10.1 ($\pm$1.1)	28.5 ($\pm$1.3)	39.4 ($\pm$1.8)
223	0.37 ($\pm$0.03)	9×10^{13}	0.99	6.3 ($\pm$0.5)	30.7 ($\pm$1.5)	42.1 ($\pm$2.0)

[a] For solid ice doped with HNO$_3$, only three temperatures are available according to the equilibrium phase diagram.[35] The quoted errors correspond to 2σ level + 5% (text). [b] $N_M \times K_{ads}(T)$ and $K(T)$ are determined from the slopes of the plots of N vs acetaldehyde concentration (eq 5). [c] ΔG^0_{ads} is obtained from eq 3. [d] ΔH^0_{ads} is derived from eq 3, assuming that ΔS^0_{ads} can be calculated from Trouton's rule.[30]

Figure 5. Plot of K as a function of $1/T$ for the different types of ice: pure ice, solid, and solid/liquid surfaces doped with HNO$_3$. For pure ice surfaces, the values of K derived from linear plots and Langmuir model (text) have been distinguished. The adsorption enthalpy is derived from the slope according to eq 3.

Figure 6. Equilibrium phase diagram of the binary system HNO$_3$–H$_2$O.[35] Also shown is the dynamic phase diagram (red lines) reported by Mahé (1999).[36]

As already observed for both acetone and ethanol,[7,23] the amounts of acetaldehyde adsorbed on solid nitric acid-doped ice are slightly lower than those obtained on pure ice (Figure 4), whatever the temperature and the concentration of HNO$_3$. This phenomenon might be explained by the presence of cracks on pure ice surfaces, whereas no cracks were observed for nitric acid-doped ice surfaces. The quantity of cracks, on pure ice, increases when decreasing the temperature down to 203 K.

Uptake on Solid/Liquid Ice Surfaces Doped with HNO$_3$. When the ice samples are prepared at ~253 K and directly cooled down to the wanted temperature, supercooled solutions form, as has been observed in our previous studies[7,23] for temperatures down to 200–210 K depending on the amount of nitric acid. As shown in Figure 5, this is in agreement with the dynamic phase diagram of the binary HNO$_3$–H$_2$O system.[36] The use of the lever rule permits us to estimate the liquid percentage in the liquid/solid phase and the nitric acid weight percentage in the liquid part (Table 2) for temperature ranging

between 203 and 253 K and for nitric acid concentration in liquid/solid ice surfaces of 0.063, 0.63, and 6.3 wt %. The liquid percentage in the liquid/solid phase increases with increasing both temperature and nitric acid concentration, as illustrated in Table 2. In the temperature range 203–243 K, the liquid part in the liquid/solid phase is less than 0.5% for ice doped with 0.063 wt % of HNO$_3$ but varies in the range 1.3–5.0% for ice doped with 0.63 wt % of HNO$_3$. Besides, the nitric acid weight percentage in the liquid phase increases from 16 to 36% when temperature increases up to 243 K and does not vary with the initial nitric acid weight percentage for a given temperature (Table 2).

The adsorption peaks, which on pure ice extended over a few seconds, spread out over few minutes for solid/liquid ice

TABLE 2: Liquid wt % in the Liquid/Solid Mixture and Nitric Acid wt % in the Liquid Phase for Temperature Ranging between 203 and 253 K and for Nitric Acid Concentrations in the Film of 0.063, 0.63, and 6.3 wt % According to the Dynamic Phase Diagram of the Binary HNO_3-H_2O System[36]

T (K)	Liquid % in the Liquid/Solid Mixture			HNO_3 wt % in the Liquid Phase		
	HNO_3 6.3 wt %	HNO_3 0.63 wt %	HNO_3 0.063 wt %	HNO_3 6.3 wt %	HNO_3 0.63 wt %	HNO_3 0.063 wt %
203	15.2	1.34	0.13	16	16	16
213	18.7	1.6	0.16	21	21	21
223	24.3	2.0	0.20	26	26	26
233	36	2.72	0.27	32	32	32
243	90	4.97	0.48	36	36	36
253	100	100	100	6.3	0.63	0.063

doped with HNO_3 (6.3 wt %) as shown in Figure 2. Note that adsorption of acetaldehyde was always reversible under our experimental conditions whatever the concentration of HNO_3. In addition, the concentration of HNO_3 in the film is not affected since in a previous study, pH−metric analysis performed on the liquid resulting from the melting of the ice film after a series of experiments showed no significant loss or increases in acid concentration.[7]

The number of acetaldehyde molecules taken up on the ice surfaces doped with HNO_3 increases significantly compared to pure ice surfaces. As observed in Figure 7, the surface coverage increases with the nitric acid concentration. At 213 K for example, temperature below the solidus line, and for low concentrations of acetaldehyde ($<1 \times 10^{13}$ molecule cm^{-3}) that

Figure 7. Adsorption isotherms of acetaldehyde at 213 K on different liquid/solid surfaces (0.063, 0.63, and 6.3 wt % of HNO_3) and comparison with that obtained on pure ice: (a) Logarithmic scale for high concentrations and (b) linear plots for acetaldehyde concentration lower than 1×10^{13} molecules cm^{-2}.

corresponds to a linear isotherm (part b of Figure 7), the amount of acetaldehyde molecules taken up on solid/liquid doped ice surfaces is 3.3 and 8.8 times higher than those measured on pure ice respectively for 0.063 and 0.63 wt % of HNO_3. For higher acetaldehyde concentration ($>1 \times 10^{14}$ molecule cm^{-3}), the number of acetaldehyde molecules taken up increases up to 2 orders of magnitude compared to pure ice surfaces, as shown in part a of Figure 7. Similar behaviors have been observed at 203, 223, 233, or 243 K.

The huge quantities of acetaldehyde taken up by nitric acid doped-ice surfaces can be explained by the dissolution of acetaldehyde in the nonhomogeneous liquid part of doped ice surfaces. For a given temperature, the amount of scavenged acetaldehyde increases with the liquid content of the film that is with the initial acid concentration (Figure 7). The enhanced uptake for acetaldehyde at these temperatures most likely results from the fact that dissolution into a liquid (where diffusion is favored compared to a solid) is more efficient than adsorption onto a solid.

The presence of a liquid solution is consistent with the adsorption/desorption cycles observed in Figure 2. Indeed, the cycles are much longer for experiments performed on nitric acid doped-ice surfaces compared to those conducted on pure ice films. We can also note from Figure 2 that the time of the adsorption/desorption processes increased with the initial nitric acid concentration, which corresponds to an increase of the amount of solution.

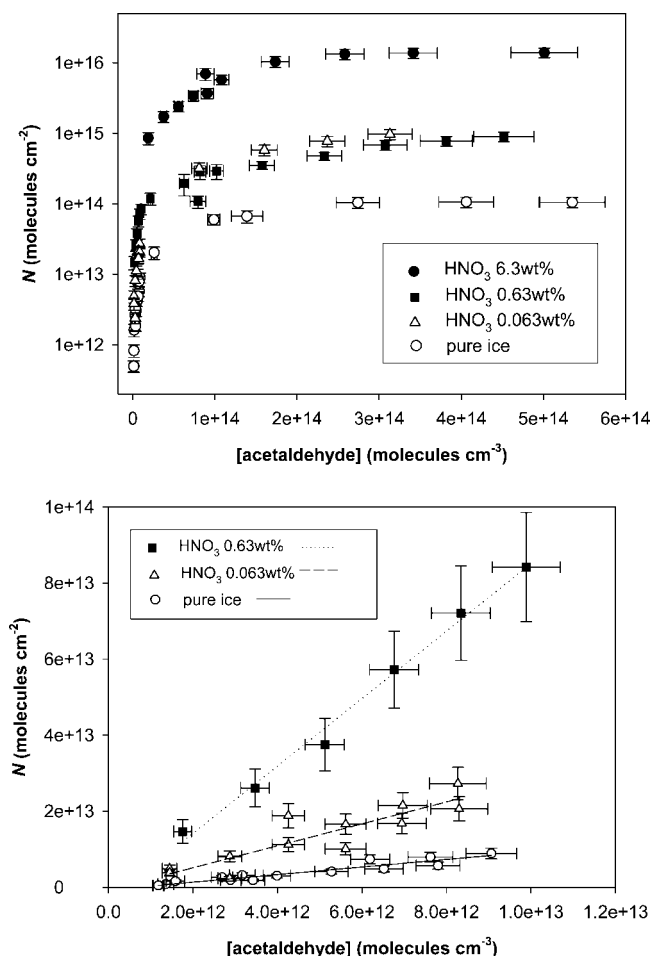Acetaldehyde is likely to dissolve in the liquid part of the films according to the Henry's law equilibrium:

$$H = \frac{[CH_3CHO]_{liq}}{P_{CH_3CHO}} \qquad (6)$$

where H is the Henry's law constant conventionally expressed in mol L^{-1} atm^{-1}, $[CH_3CHO]_{liq}$ is the acetaldehyde concentration in the liquid (in mol L^{-1}), P_{CH_3CHO} is the partial pressure of acetaldehyde over the liquid phase (in atm).

Such a hypothesis is consistent with the fact that N first increases linearly with the acetaldehyde gas-phase concentration (part b of Figure 7). In such a case, a pseudo Henry's law constant H^* can be derived by combining eq 2 and eq 4, which leads to

$$H^* = \frac{[CH_3CHO]_{liq}}{P_{CH_3CHO}} = \frac{1.013 \times 10^6 N_M K_{ads}}{epRT} \qquad (7)$$

where $N_M \times K_{ads}$ is the slope of the adsorption isotherms in centimeters, e is the thickness of the film expressed in

Uptake Measurements of Acetaldehyde

J. Phys. Chem. A, Vol. 113, No. 17, 2009 **5097**

TABLE 3: Values of $N_M \times K_{ads}(T)$, $K(T)$, ΔG^0_{ads}, and ΔH^0_{ads} for Different Types of Liquid/Solid Ice Surfaces at 203, 213, 223, 233, 243, and 253 K[a]

T (K)	$N_M \times K_{ads}{}^b$ (cm)	R^2	$K \times 10^{-8b}$ (dimensionless)	$-\Delta G^0_{ads}{}^c$ (kJ mol^{-1})	$-\Delta H^0_{ads}{}^d$ (kJ mol^{-1})	$H*^e$ (M atm^{-1})
			Liquid/Solid Ice Doped with 0.063 wt % of HNO$_3$			
203	14.8 (±1.6)	0.99	251 (±27)	21.8 (±0.9)	32.1 (±1.4)	6.5 (±0.9) × 10^4
213	3.3 (±0.3)	0.99	56 (±5)	25.5 (±1.2)	36.4 (±1.7)	8.2 (±1.2) × 10^3
223	1.2 (±0.1)	0.99	20 (±2)	28.6 (±1.4)	40.0 (±1.8)	2.2 (±0.3) × 10^3
233	0.62 (±0.05)	0.99	10 (±1)	31.1 (±1.5)	43.0 (±2.1)	440 (±40)
243	0.45 (±0.04)	0.99	7.7 (±0.6)	33.1 (±1.6)	45.5 (±2.2)	99 (±12)
			Liquid/Solid Ice Doped with 0.63 wt % of HNO$_3$			
213	8.37 (±0.21)	0.99	142 (±14)	23.8 (±1.1)	34.7 (±1.6)	2.8 (±0.2) × 10^3
223	1.26 (±0.12)	0.98	21.4 (±2.1)	28.5 (±1.3)	39.9 (±1.9)	229 (±22)
233	1.14 (±0.09)	0.99	19.4 (±1.6)	29.9 (±1.4)	41.8 (±2.0)	145 (±9)
243	0.65 (±0.07)	0.99	11.0 (±1.1)	32.4 (±1.5)	44.8 (±2.1)	29 (±2)
253	0.35 (±0.06)	0.99	5.9 (±1.0)	35.0 (±1.5)	47.9 (±2.1)	-

[a] The linear plots were obtained for acetaldehyde concentrations lower than 5×10^{14} molecule cm^{-2}. The quoted errors correspond to 2σ level + 5% (text). [b] $N_M \times K_{ads}(T)$ and $K(T)$ are determined from the slopes of the plots of N vs acetaldehyde concentration (eq 5). [c] ΔG^0_{ads} is obtained from eq 3. [d] ΔH^0_{ads} is derived from eq 3 assuming that ΔS^0_{ads} can be calculated from Trouton's rule.[30] [e] The values of $H*$ are calculated according to eq 5 assuming that the thickness of our experimental liquid/ice surfaces is 100 μm.

micrometers, p is the fraction of liquid given by the phase diagram (Table 2), and R is the gas constant in J mol^{-1} K^{-1}.

This equation was considered to estimate $H*$ under our experimental conditions and the results are shown in Table 3. Calculations were made for a film thickness of 100 μm, which corresponds to the typical value found by weighting the solution at the end of an experiment (Experimental Section). The values of $H*$ were derived assuming that the liquid part of the film was totally accessible to the gaseous acetaldehyde. For 6.3 wt % of HNO$_3$, the isotherm is not linear in the studied gaseous concentration range, so that any thermodynamic parameter can not derive.

Because adsorption of acetaldehyde on solid ice competes with dissolution in the supercooled liquid phase under our experimental conditions, eq 7 was corrected as follows:

$$H* = \frac{[CH_3CHO]_{liq}}{P_{CH_3CHO}}$$

$$= \frac{1.013 \times 10^6[(N_M K_{ads})_{liq} - (N_M K_{ads})_{solid}]}{epRT} \quad (8)$$

where $(N_M K_{ads})_{liq}$ corresponds to the supercooled mixtures and $(N_M K_{ads})_{solid}$ refers to the corresponding doped solid ice surfaces for 203–223 K and to the pure ice surfaces for $T \geq 233$ K.

The variation of Henry's law constants as a function of temperature can be expressed with a van't Hoff equation; therefore ln $H*$ has been plotted as a function of $1/T$ in Figure 8. Although our Henry's law constants refer to the partitioning of acetaldehyde between the gas phase and a water–nitric acid solution in the liquid phase, it is tempting to compare our values of $H*$ to those of the usual gas/water equilibrium obtained at 298 and 273 K, that is 13 and 77 mol L^{-1} atm^{-1} respectively and extrapolated to our temperature range.[37]

Figure 8 shows that $H*$ values for doped films are significantly lower than those obtained for pure water. In addition, $H*$ values seem to decrease with nitric acid concentration, at least for the concentration range used in this study. These results are in good agreement with the observations of Michelsen et al.,[38] who studied the dissolution of acetaldehyde in cold sulfuric acid solutions. Indeed, these authors found that acetaldehyde is considerably less soluble in moderately acidic solutions (less than 45–50 wt %) than in pure water and that its solubility
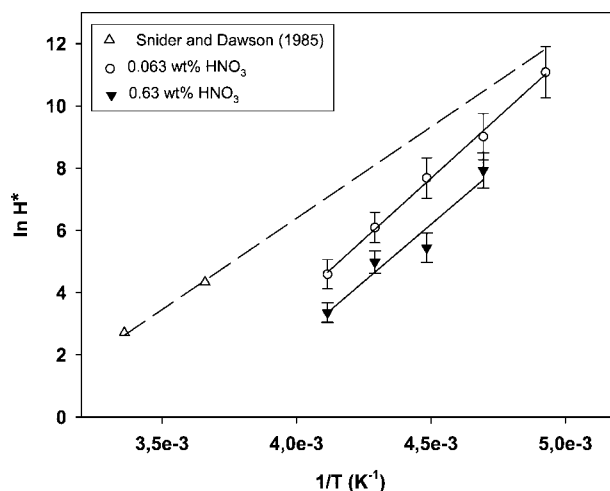
Figure 8. Plot of ln $H*$ as a function of $1/T$. Our extrapolated values on 0.063 and 0.63 wt % nitric acid-doped surface are compared with those of Snider and Dawson (1985) obtained for pure liquid water surfaces.[37]

first decreases with acid concentration. It is only for acid concentrations larger than about 70 wt % that the solubility is larger than that in pure water. A similar behavior was found by Esteve and Nozière,[39] who showed that, at 298 K, the solubility of acetaldehyde in sulfuric acid solutions is minimal at an acid concentration of about 25 wt %. This behavior was not observed for both acetone and ethanol because they are much more soluble in the aqueous phase.

Atmospheric Implications. The fraction of A $f_{A,cirrus}$ scavenged by ice surfaces contained in a cirrus cloud can be estimated as follows:

$$f_{A,cirrus} = \frac{[A]_{solid}}{[A]_g + [A]_{solid}} = \frac{N_M \times K_{ads} \times D_{cirrus}}{1 + N_M \times K_{ads} \times D_{cirrus}} \quad (9)$$

where D_{cirrus} is the surface area densities of ice ranging between 1×10^{-4} and 1×10^{-7} cm^2 cm^{-3}.[40]

Even in the densest ice clouds and in the most favorable case, that is $T = 203$ K, 0.02% of acetaldehyde could be adsorbed on pure ice surfaces. The amount of OVOCs such as acetaldehyde scavenged by pure ice is therefore negligible as shown in this work and in previous laboratory studies.[17–22]

The estimated Henry's law constants can be used to evaluate the partitioning of oxygenated VOCs between the gas and liquid phases inside a supercooled cloud at temperatures close to 230−240 K. Assuming that both mass accommodation and gas diffusion do not limit the rate of gas uptake and therefore that the equilibrium between the gas and supercooled liquid phase is rapidly reached, the fraction of A in the aqueous phases ($f_{A,aq}$) can be estimated as follows:[40]

$$f_{A,aq} = \frac{[A]_{aq}}{[A]_g + [A]_{aq}} = \frac{H^* R L_{wc} T}{1 + H^* R L_{wc} T} \tag{10}$$

where R the ideal gas constant (in L atm mol^{-1} K^{-1}), L_{wc} the dimensionless liquid water content of the supercooled cloud, and T the cloud temperature (in K).

In situ measurements in deep convective clouds have shown that the supercooled droplets can reach a median volume diameter of 17 μm and amount to 1.8 g m^{-3} [5] corresponding to $L_{wc} = 1.80 \times 10^{-6}$, which is approximately 1 order of magnitude higher than the value usually reported for tropospheric clouds.[41] On the basis of this value of L_{wc} and on the values of H^* derived from our experiments (442 M atm^{-1} at 233 K) or on the extrapolated values of H^* from its experimental determination at 273 K (2960 M atm^{-1} at 233 K), 1.5−9.2% of acetaldehyde may be scavenged by supercooled liquid droplets of convective clouds. This phenomenon is then non-negligible, even if the uptake of acetaldehyde in convective clouds is less efficient than those estimated for more soluble OVOCs such as methanol (f_{aq} = 0.50), ethanol (f_{aq} = 0.76), formic acid (f_{aq} = 0.97), acetic acid (f_{aq} = 0.98), and formaldehyde (f_{aq} = 0.98).[7]

References and Notes

(1) Heymsfield, A. J.; Sabin, R. M. *J. Atmos. Sci.* **1989**, *46*, 2252.
(2) Seinfeld, J. H.; Pandis, S. N. *Atmospheric Chemistry and Physics*; Wiley: New York, 1998.
(3) Hoyle, C. R.; Luo, B. P.; Peter, T. *The origin of high ice crystal number densities in cirrus clouds* **2005**, *7*, 2568.
(4) Sassen, K.; Liou, K.-N.; Kinne, S.; Griffin, M. *Science* **1985**, *227*, 410.
(5) Rosenfeld, D.; Woodley, W. L. *Nature* **2000**, *405*, 440.
(6) Kley, K. *Science* **1997**, *276*, 1043.
(7) Kerbrat, M.; Le Calvé, S.; Mirabel, P. *J. Phys. Chem. A* **2007**, *111*, 925.
(8) Krämer, M.; Schiller, C.; Ziereis, H.; Ovarlez, J.; Bunz, H. *Tellus Series B - Chemical and Physical Meteorology* **2006**, *58B*, 141.
(9) Stuart, A. L.; Jacobson, M. Z. *J. Geophys. Res.* **2003**, 108. doi: 10.1029/2001JD001408.
(10) Laaksonen, A.; Hienola, J.; Kulmala, M.; Arnold, F. *Geophys. Res. Lett.* **1997**, *24*, 3009.
(11) Arnold, F.; Bürger, V.; Droste-Fanke, B.; Grimm, F.; Krieger, A.; Schneider, J.; Stilp, T. *Geophys. Res. Lett.* **1997**, *24*, 3017.
(12) Mari, C.; Saüt, C.; Jacob, D.; Ravetta, F.; Anderson, B.; Avery, M. A.; Blake, D. R.; Brune, W. H.; Faloona, I.; Gregory, G. L.; Heikes, B. G.; Sachse, G. W.; Sandholm, S. T.; Singh, H. B.; Talbot, R. W.; Tan, D.; Vay, S. *J. Geophys. Res* **2003**, 108D2, 8229.
(13) Singh, H.; Chen, Y.; Staudt, A.; Jacob, D.; Blake, D.; Heikes, B.; Snow, J. *Nature* **2001**, *410*, 1078.
(14) Singh, H.; Chen, Y.; Tabazadeh, A.; Fukui, Y.; Bey, I.; Yantosca, R.; Jacob, D.; Arnold, F.; Wohlfrom, K.; Atlas, E.; Flocke, F.; Blake, D.; Heikes, B.; Snow, J.; Talbot, R.; Gregory, G.; Sachse, G.; Vay, S.; Kondo, Y. *J. Geophys. Res.* **2000**, *105*, 3795.
(15) Abbatt, J. P. D. *Chem. Rev.* **2003**, *103*, 4783.
(16) Kärcher, B.; Voigt, C. *Geophys. Res. Lett.* **2006**, *33*, L08806.
(17) Dominé, F.; Rey-Hanot, L. *Geophys. Res. Lett.* **2002**, *29*, 1873.
(18) Peybernès, N.; Le Calvé, S.; Mirabel, P. *J. Chem. Phys. B* **2004**, *108*, 17425.
(19) Peybernès, N.; Marchand, C.; Le Calvé, S.; Mirabel, P. *Phys. Chem. Chem. Phys.* **2004**, *6*, 1277.
(20) Picaud, S.; Hoang, P. N. N.; Peybernès, N.; Le Calvé, S.; Mirabel, P. *J. Chem. Phys.* **2005**, *122*, 194707.
(21) Sokolov, O.; Abbatt, J. P. D. *J. Phys. Chem. A* **2002**, *106*, 775.
(22) Winkler, A. K.; Holmes, N. S.; Crowley, J. N. *Phys. Chem. Chem. Phys.* **2002**, *4*, 5270.
(23) Journet, E.; Le Calvé, S.; Mirabel, P. *J. Phys. Chem. B* **2005**, *109*, 14112.
(24) Hudson, P. K.; Zondlo, M. A.; Tolbert, M. A. *J. Phys. Chem. A* **2002**, *106*, 2882.
(25) Taylor, G. *Proc. R. Soc. London* **1953**, *219*, 186.
(26) Kemball, C. *Proc. R. Soc. London, Ser. A* 1946, *187*, 73.
(27) Kemball, C.; Rideal, E. K. *Proc. R. Soc. London, Ser. A* 1946, *187*, 53.
(28) Carmichael, H. *J. Chem. Educ.* 1976, *53*, 695.
(29) Bartels, T.; Eichler, B.; Zimmermann, P.; Gäggeler, H. W.; Ammann, M. *Atmos. Chem. Phys.* **2002**, *2*, 235.
(30) Atkins, P. W. *Physical Chemistry*, 5th ed.; W. H. Freeman, Ed.; Oxford University Press: New York, 1994.
(31) Lyman, W. J.; Reehl, W. F.; Rosenblatt, D. H. *Handbook of Chemical Property Estimation Methods. Environmental Behavior of Organic Compounds*; Washington D.C., 1990; Vol. 2.
(32) Gao, R. S.; Popp, P. J.; Fahey, D. W.; Marcy, T. P.; Herman, R. L.; Weinstock, E. M.; Baumgardner, D. G.; Garrett, T. J.; Rosenlof, K. H.; Thompson, T. L.; Bui, P. T.; Ridley, B. A.; Wofsy, S. C.; Toon, O. B.; Tolbert, M. A.; Karcher, B.; Peter, T.; Hudson, P. K.; Weinheimer, A. J.; Heymsfield, A. J. *Science* **2004**, *303*, 516.
(33) Heymsfield, A. J.; Knollenberg, R. G. *J. Atmos. Sci.* **1972**, *29*, 1358.
(34) Gayet, J. F.; Febvre, G.; Brogniez, G.; Chepfer, H.; Renger, W.; Wendling, P. *J. J. Atmos Sci.* **1996**, *53*, 126.
(35) Beyer, K. D.; Hansen, A. R. *J. Phys Chem A* **2002**, *106*, 10275.
(36) Mahé, F. Etude des Diagrammes de Phases du Système HNO$_3$/H$_2$SO$_4$/H$_2$O: Composition et Mécanismes de Formation des Aérosols Stratosphériques (Study of the Ternary Phase Diagrams H$_2$SO$_4$/HNO$_3$/H$_2$O: Composition and Formation Mechanisms of Stratospheric Aerosols, Ph.D. Thesis, Université d'Orléans, 1999.
(37) Snider, J. R.; Dawson, G. A. *J. Geophys. Res.* **1985**, *90-D2*, 3797.
(38) Michelsen, R. R.; Ashbourn, S. F. M.; Iraci, L. T. *J. Geophys. Res.* **2004**, *109*, >D23205.
(39) Esteve, W.; Nozière, B. *J. Phys. Chem. A* **2005**, *109*, 10920.
(40) Solomon, S.; Borrmann, S.; Garcia, R. R.; Portmann, R.; Thomason, L.; Poole, L. R.; Winker, D.; McCormick, M. P. *J. Geophys. Res.* **1997**, *102*, 21411.
(41) Kolb, C. E.; Worsnop, D. R.; Zahniser, M. S.; Davidovits, P.; Hanson, D. R.; Ravishankara, A. R.; Keyser, L. F.; Leu, M. T.; Williams, L. R.; Molina, M. J.; Tolbert, M. A. Laboratory Studies of Atmospheric Heterogeneous Chemistry. In *Advances in Physical Chemistry Series*; Barker, J. R., Ed.; World Scientific: Singapore, 1995; Vol. 3, p 771.